Opto-Electronics Review 28 (2020) 182-190

PAN POLISH ACADEMY OF SCIENCES

Opto-Electronics Review

journal homepage: http://journals.pan.pl/opelre

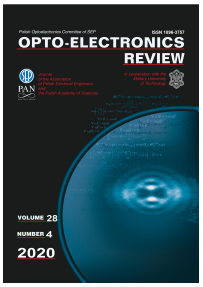

Structural, morphological and photoluminescent properties of annealed ZnO thin layers obtained by the rapid sol-gel spin-coating method

M. Sypniewska[a], R. Szczesny[b], P. Popielarski[c], K. Strzalkowski[a], B. Derkowska-Zielinska[a*]

[a] Institute of Physics, Faculty of Physics, Astronomy and Informatics, Nicolaus Copernicus University in Torun, 5 Grudziadzka St., Torun 87-100, Poland

[b]Faculty of Chemistry, Nicolaus Copernicus University in Torun, 7 Gagarina St., Torun 87-100, Poland

[c]Institute of Physics, Kazimierz Wielki University in Bydgoszcz, 2 Powstańców Wielkopolskich St., 85-090, Bydgoszcz, Poland

Article info

Article history:
Received 02 Jun. 2020
Received in revised form 27 Aug. 2020
Accepted 31 Aug. 2020

Keywords:
FTIR and Raman spectroscopies, photoluminescence, SEM, XRD, ZnO thin films.

Abstract

ZnO thin layers were deposited on p-type silicon substrates by the sol-gel spin-coating method and, then, annealed at various temperatures in the range of 573–873 K. Photoluminescence was carried out in the temperature range of 20–300 K. All samples showed two dominant peaks that have UV emissions from 300 nm to 400 nm and visible emissions from 400 nm to 800 nm. Influence of temperature on morphology and chemical composition of fabricated thin layers was examined by XRD, SEM, FTIR, and Raman spectroscopy. These measurements indicate that ZnO structure is obtained for samples annealed at temperatures above 573 K. It means that below this temperature, the obtained thin films are not pure zinc oxide. Thus, annealing temperature significantly affected crystallinity of the thin films.

1. Introduction

In recent years, thin layers of zinc oxide (ZnO) have been widely studied due to their potential applications in optoelectronics. ZnO is an n-type semiconductor because of the presence of oxygen gaps and additional donors in the network, i.e., interstitial Zn atoms. This compound occurs mainly in the form of hexagonal structures of wurtzite [1-4]. In this structure, four anions, which are located in the corners of tetrahedron, surround each cation, and similarly each anion is adjacent to four cations. A ZnO unit cell consists of four atoms: two oxygen and two zinc. The volume of such a cell is of about 47.6 Å^3. The values of the network parameters, which characterize a given semiconductor, depend on the concentration of free electrons, impurities and defects, as well as on temperature [5]. The ratio of *c/a* network parameters is of about 1.60 for an ideal ZnO wurtzite structure [1]. Other forms of zinc oxide are zinc blende and cubic rocksalt. In the first case, the growth of ZnO must be forced by the substrate crystallographic system. Whereas in the case of cubic rocksalt, the ZnO structure is created only by applying high pressures.

As mentioned above, ZnO is widely used in optoelectronics, mainly due to a wide energy band gap of about 3.3 eV and high exciton binding energy [1,2]. Additionally, it has high thermal conductivity of 50 W/mK, and, due to its structure, the largest piezoelectric properties among semiconductors [6,7]. Zinc oxide deposited on amorphous or Si substrates usually forms a polycrystalline layer without being ordered in the film plane [8]. ZnO is also used for the production of oxide varistors [4] allowing voltage limitation. Additionally, it can be used as a gas sensor because various gases can significantly affect the electrical conductivity of the ZnO surface [3]. This is mainly due to the presence of oxygen vacancies in zinc oxide. For this reason, highly doped to the n-type, using for example Al or Ga, can be used to produce transparent high conductive oxide (TCO) [9,10]. Zinc oxide was also doped with Cu, Ag and Bi and its structural, optical and nonlinear optical properties were studied [11,12]. Some research groups also used ZnO nanoparticles for improving the

*Corresponding author at: beata@fizyka.umk.pl

https://doi.org/10.24425/opelre.2020.134460

nonlinear optical response of some polymers [13]. ZnO can also be used to fabricate transparent thin-film transistors. Current research gives hope for the use of zinc oxide in the rapidly developing optoelectronics, in the field of UV and blue light. At the same time, work is underway on the use of ZnO for the production of a laser diode and a light emitting diode [14]. It should be mentioned that the photoluminescence of ZnO usually occurs in two emission bands. The first band is associated with the energy gap (band-band recombination) of around 380 nm, while the second one, in the range of about 450–700 nm, can be associated with oxygen defects [1,15-17].

ZnO thin layers can be obtained using various techniques, e.g., PLD (pulsed laser deposition), MS (magnetron sputtering), MOCVD (metal organic chemical vapor deposition), spin- and dip-coating [18-21], as well as spray pyrolysis, electrochemical deposition, etc. [22-24]. The sol-gel spin-coating method is extensively used because of a relatively easy procedure, simple deposition equipment and low cost. It should be mentioned that an expensive vacuum system does not have to be used in this technique. In addition, this method can be used to cover a large surface of uniform thickness and ensures easy doping of the film [20].

Here, we show the results regarding the structural, morphological and photoluminescent properties of thin films fabricated from zinc acetate precursor on a silicon substrate using XRD, SEM, FTIR, Raman, and photoluminescence spectroscopies. The studied layers were made using the sol-gel spin-coating technique by a novel process in which the sol was obtained immediately without having to wait 24 hours to prepare thin films, as described in other publications [25,26]. This fact results in a faster and easier production of good quality ZnO thin layers. Then, these samples were annealed at 393 K, 573 K, 673 K, 773 K, and 873 K. We show that annealing temperature significantly affected crystallinity of the studied thin layers, as well as influenced physical properties of the fabricated films.

2. Experimental

2.1 Sol-gel process

Sol-gel is a wet chemistry method extensively used for production of different solid materials in the form of coatings, thin films, fibers, or nanometric powders. Metal oxides products are fabricated in the hydrolysis-condensation processes from the molecular precursor. It involves a conversion of monomers resulted in a colloidal suspension (sol) and a further gelation leading to a formation of continuous liquid integrated network (gel). In the case of films, the homogeneous precursor fluid can be deposited directly on substrate and two methods: spin- or dip-coating are very often utilized for this purpose. Removing of the solvent during deposition, subsequent drying and final thermal treatment allows to form oxide coatings [27-29]. Thin layers of zinc oxide are often fabricated in a sol-gel process where aqueous solutions of various inorganic or organic zinc salts are dissolved in alcoholic solvents [30].

There are many described in the literature zinc-containing precursors of ZnO films such as perchlorates and acetates [31,32], chlorides [31] or nitrates [33]. However, it should be mentioned that ZnO films made from a zinc acetate precursor exhibit a smoother surface than by using other salts. Therefore, zinc acetate dihydrate [29,31,32] has found a wide application in the production of this type of layers. Advantages of using zinc acetate dihydrate derived from its solubility in water and organic solvents such as ethanol or isopropanol and easy removal of acetate anions during the thermal treatment. Beside the metal precursor, the presence of amine additives (stabilizers) in the sol-gel process are essential. These reagents react with the precursor and, facilitating the formation of complexes, act as chelating ligands which prevent a rapid precipitation, and support the formation of stable solutions. The most common stabilizers for zinc oxide are monoethanolamine (MEA) and diethanolamine (DEA). The more stable, transparent and homogeneous sols are prepared using MEA which has a lower boiling point (443 K) than DEA (i.e., 543 K). In addition, MEA promotes to remove organic substances more efficiently during the thermal film processing [34].

The sequence of interrelated chemical reactions of hydrolysis of the metal precursor and condensation leads to the formation of a metal oxide network [35]. Zinc acetate dihydrate ($Zn(CH_3COO)_2{\cdot}2H_2O$) dissociate and mono-acetate ($(CH_3COO)Zn^+$ ions are present in the solution. These ions can react with monoethanolamine resulting in a formation of chelated species. The amine is in competition with acetate groups complexing Zn^{2+} ions. The existing in the system nucleophilic species such as MEA, CH_3COO^- and OH^- compete for the Zn^{2+} sites. The zinc-oxo-acetate oligomers are formed as a result of the attack of the hydroxy group and hydrolysis of Zn–CH_3COO or Zn–MEA soluble complexes. The progressive condensation of the hydrolyzed moieties generates the formation of colloids [36]. The scheme of the reactions taking place during the particular sol-gel process are illustrated in Fig. 1.

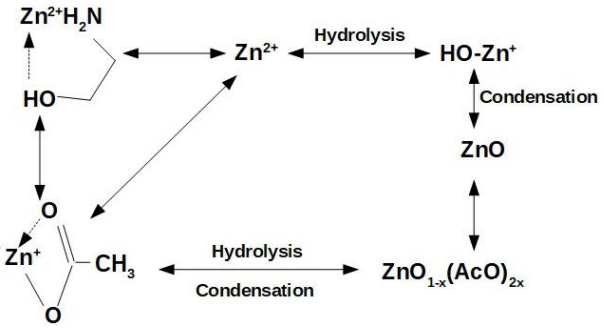

Fig. 1. The reaction scheme for a zinc acetate - monoethanolamine sol-gel process.

2.2 Film deposition

To prepare sol solution, the zinc acetate dihydrate (Merck) and monoethanolamine (MEA, Sigma-Aldrich, 99.5%) were added to isopropanol alcohol (Chempur, pure p.a.). The solution was then slowly heated to 343 K with continuous stirring and elevated at this temperature for 60 min. ZnO layers were deposited on a p-Si substrate

using a spin-coating method (with 2000 r/min for 30 s). The process was repeated 5 times. However, to evaporate the solvent from the layer, we dried each of the newly formed films at 393 K for 10 min. Finally, we put the sample into the furnace and annealed it in the ambient atmosphere at a selected temperature (i.e., 573 K, 673 K, 773 K, or 873 K) for 1 hour and afterwards the furnace was slowly cooled to room temperature.

2.3 *Characterization of thin layers*

The crystalline structure of ZnO thin layers was examined by an X-ray diffraction (XRD) method. XRD diffractograms were recorded using a Philips X'Pert diffractometer (CuKα radiation, $\lambda = 1.5404$ Å) in the 2Θ range from 20° to 70°. Whereas the topography of ZnO thin films deposited and annealed at different temperatures was characterized by a scanning electron microscope (SEM, Quanta 3D FEG, EHT = 30 kV, HV mode, SE). The Raman spectra were recorded using Raman spectrometer (Senterra by Bruker Optik) in the spectral range of 200–1500 cm^{-1}, where a laser of 532 nm (10 mW) has been used as a source of excitation. The FTIR spectra were measured using FT-IR Vertex 70 V with a Hyperion 1000/2000 microscope by Bruker Optik from 200 cm^{-1} to 4000 cm^{-1}. The luminescent properties of prepared thin layers on Si substrates were registered by the system consisting of He-Cd laser (Omnichrom, 325 nm, 20 mW), SPM-2 monochromator, photomultiplier, cryostat, and temperature controller. This configuration was used for a temperature-dependent luminescence measurement in the range of 20–300 K.

3. Results and discussion

The XRD patterns of studied thin films deposited on a Si substrate and annealed at various temperatures in the range of 373–873 K are shown in Fig. 2(a). One can see that the XRD pattern showed reflections which correspond to the following planes (100), (002), (101), (102), (110), (103), (200), (112), and (201) at 2Θ = 32.38, 34.98, 36.88, 48.15, 57.15, 63.47, 67.11, 68.32, and 69.75, respectively. It should be mentioned that among studied samples they are only visible for thin layers that are annealed from 573 K. For a sample dried at 393 K, typical ZnO peaks are not observed. This suggests that we are dealing with an amorphous structure.

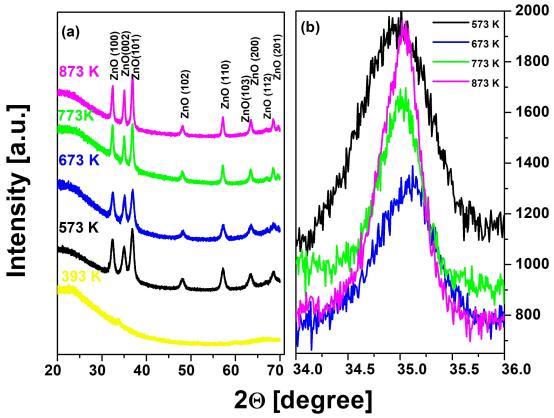

Fig. 2. XRD pattern of studied thin films annealed at various temperatures (a). XRD (002) peak of studied thin films (b).

From Fig. 2 one can see that the increase in the annealing temperature caused the narrowing of the peak. It should be noted that the growth of ZnO layers with orientation (002) is kinetically preferred. This could mean that the highest density of zinc atoms can be found exactly along this plane [37]. This indicates that the preferred orientation of the ZnO layer is along the c-axis and ZnO thin film has a wurtzite structure [38].

The effect of the temperature dependence on full width at half maximum (FWHM) of selected XRD patterns is presented in Fig. 3. In general, it can be observed, that as the annealing temperature increases, the FWHM value decreases for all the observed peaks indicating the increase of grains size.

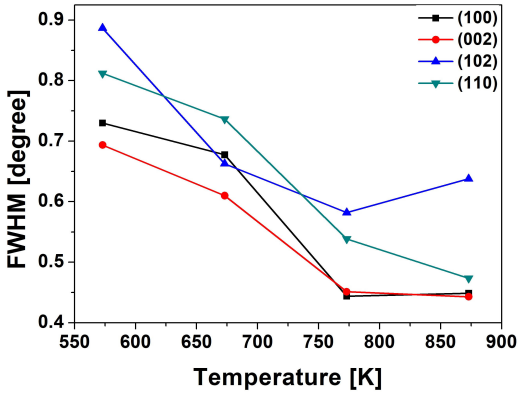

Fig. 3. Temperature dependence of FWHM of selected XRD peaks.

To calculate the crystallite size of prepared thin films, we can use the well-known Debye-Scherrer equation:

$$D = \frac{0.9\lambda}{\beta cos\Theta}, \quad (1)$$

where λ is the X-ray wavelength, β is the FWHM of the XRD peak and Θ is the Bragg diffraction angle.

We found that the estimated particle size, determined from (002) peak has a nano value that is between 17 nm (for sample annealing at 573 K) and 35 nm (for 873 K). The values of the calculated grain size are in accordance with the literature [39]. The values of the lattice constants (i.e., *a* and *c*) calculated from (100) and (002) planes, as well as the *c*/*a* ratio are presented in Table 1. It is well known that the *c*/*a* ratio is equal to 1.63 for the wurtzite structure. It can be seen from Table 1 that the estimated values are in accordance with the ideal value (i.e., 1.63).

Table 1
Structural parameters of investigated thin layers, where *a* and *c* are the lattice constants, ε is the strain, and σ is the residual stress.

T	(hkl)	2Θ (hkl) [degree]	$a_{(100)}$ [Å]	$c_{(002)}$ [Å]	*c*/*a*	ε [%]	σ [GPa]
573 K	002 100	35.148 32.352	- 3.193	5.102 -	1.597	-2.02	4.70
673 K	002 100	35.020 32.481	- 3.181	5.120 -	1.609	-1.67	3.89
773 K	002 100	34.892 32.619	- 3.168	5.138 -	1.610	-1.32	3.07
873 K	002 100	34.892 32.620	- 3.165	5.138 -	1.620	-1.32	3.07

Therefore, it can be assumed that these crystallites have a crystal structure with a low concentration of structural defects.

Information about the structural characteristics of studied thin layers can be obtained from strain (ε) and residual stress (σ) using the following equations [40-42]:

$$\varepsilon = \frac{c-c_0}{c_0} 100\% , \quad (2)$$

and

$$\sigma = \frac{2c_{13}^2 - c_{33}(c_{11}+c_{12})}{2c_{13}} \frac{c-c_0}{c_0} , \quad (3)$$

where c_0 is the unstrained lattice parameter of bulk ZnO ($c_0 = 5.207$ Å [40]), and the stiffness constants for ZnO single crystals are as follows: $c_{11} = 208.8$ GPa, $c_{33} = 213.8$ GPa, $c_{12} = 119.7$ GPa, $c_{13} = 104.2$ GPa [40,43].

Taking into account the above values for c_{ij} coefficients, the residual stress can be determined from:

$$\sigma = -233 \frac{c-c_0}{c_0}. \quad (4)$$

It should be mentioned that the positive σ values indicate tensile stress resulting from stretching the crystal size and this means that the lattice constant was reduced compared to the no-stress sample [41]. From the values presented in Table 1, it can be seen, that the strain (ε) is tensile in studied layers.

Figure 4(a) shows Raman plots for prepared thin layers annealed at various temperatures. Whereas Figure 4(b) presents Raman spectrum of ZnO thin film annealed at 873 K. It should be mentioned that zinc oxide has a wurtzite structure with a symmetry of the C_{6V}^4 point group [44,45]. Therefore, the group theory predicts that there are two modes for each of A_1, E_1, E_2, and B_1. However, only two B_1 modes are not active in Raman. From these figures, one can see that the Raman scattering from the ZnO vibrational modes are dominated by two peaks at about 99 cm^{-1} and 436 cm^{-1} that are assigned to the E_2(low) and E_2(high) optical phonons of the ZnO crystal, respectively. Low frequency E_2 mode is associated with vibrations of the heavy Zn subnet. Whereas the high frequency E_2 mode includes only oxygen atoms [46]. Peak with a weak intensity at about 434 cm^{-1} is characteristic of the Raman mode of the hexagonal wurtzite structure. The shift from 443 cm^{-1} to 434 cm^{-1} was due to the tensile strain in the layers [46]. The E_1(LO) positioned at about 583 cm^{-1} is attributed to the formation of the defects, such as a vacancy of oxygen or interstitial Zn atoms. We found that the frequencies of measured optical modes in studied ZnO thin films (i.e., E_2(low) – 99 cm^{-1}, E_2(high) – 436 cm^{-1}, A_1(TO) – 380 cm^{-1}, A_1(LO) – 574 cm^{-1}, E_1(TO) – 405 cm^{-1}, and E_1(LO) – 583 cm^{-1}) are in good agreement with those published elsewhere [34,47]. It should also be noted that peaks at 290, 302, 520, 620, and 960 cm^{-1} are silicon vibration modes.

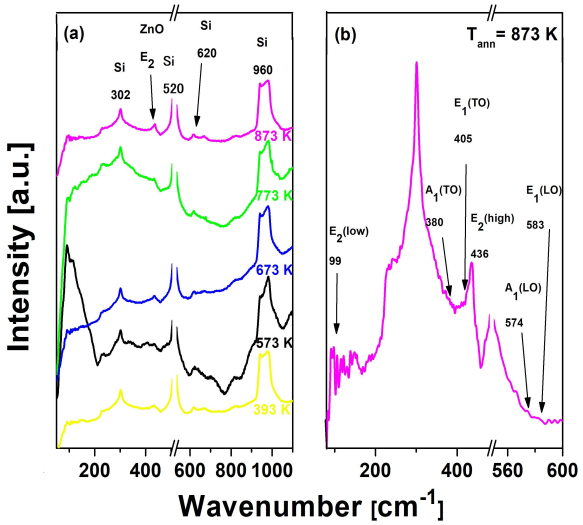

Fig. 4. Raman spectra of studied thin layers (a). Raman spectrum of ZnO thin film annealed at 873 K (b).

FTIR spectra registered for thin films annealed at temperatures from the range of 573 K–873 K are presented at Fig. 5. Moreover, the peak positions and the assigned vibration modes are summarized in Table 2.

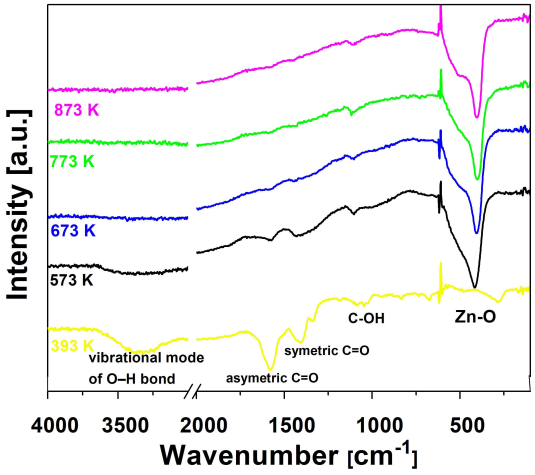

Fig. 5. FTIR spectra of thin films annealed at various temperatures.

Table 2
FTIR vibration modes (in cm^{-1} units) detected in studied thin films.

Annealing temperature	393 K	573 K	673 K	773 K	873 K
Zn–O	-	419	411	402	411
	-	523	516	513	511
ν C–OH	1050	1093	1085	1110	1102
$\nu_{Symmetric}$ C=O	1401	1426	1434	1443	-
$\nu_{Asymmetric}$ C=O	1568	1576	1584	1590	-
ν O–H	3100 - 3650	3000 - 3620	-	-	-

The peaks derived from the stretching vibration of ZnO are visible in the spectrum of samples annealed at temperatures 573 K (410/520 cm^{-1}) and higher. Below this temperature, peaks from others functional groups are dominant. The broad one registered between 3600–3000 cm^{-1} can be a result of overlapping of stretching vibrations of N–H (MEA) and O–H (absorbed water compound). The peaks visible at ~1570 cm^{-1} and ~1420 cm^{-1} were assigned to the asymmetric and symmetric stretching

vibrations of C=O of the acetate group, respectively [39]. Additional peaks registered at lower temperatures between 1040 and 1100 cm^{-1} arise both from both amine and acetate anions.

SEM micrographs of studied thin layers annealed at various temperatures at magnification 200k are shown in Fig. 6. An irregular morphology is obtained when the annealing temperature is low (i.e., 573 K and for unheated layers). Thin layers annealed at 673 K, 773 K and 873 K present similar morphological characteristics. Their morphology shows inhomogeneous, dense, agglomerated particles. SEM micrograph shows that the average grain size increases with increasing annealing temperature. This can be taken as the result of a coalescence process that effectively changes the thin film topography. The increase in grain size visible in the SEM micrographs is consistent with the results calculated from XRD measurements. Whereas Figure 7 presents the SEM micrographs of studied thin layers annealed at two highest temperatures at magnification 10k. We found that in the micro level, the films obtained at 573 K layers were continuous with some hogback-like structures. However, increasing the annealing temperature significantly reduces the size of the ridges up to 773 K [see Fig. 7(a)]. And finally, at the highest annealing temperature cracks in the layer are occurring [Fig. 7(b)].

Figure 8 presents the photoluminescence (PL) spectra of prepared thin layers annealed at different temperatures which were examined by an excitation wavelength of 325 nm at 20 K. One can see that all samples show two dominant peaks that have a UV emission from 350 nm to 450 nm, and visible emission at 480 nm to 800 nm. PL spectra of studied layers demonstrate strong emission focused around 380 nm due to the emission of a free exciton (resulting from the recombination of free excitons in the exciton-exciton collision process). Studied layers also present a strong and wide yellow-orange emission. This band discloses the recombination of a photo-generated holes with electrons belonging to individually ionized oxygen free sites. It is well known that pure zinc oxide can reveal green and/or orange luminescence which depends on the growth temperature, as well as the access of oxygen

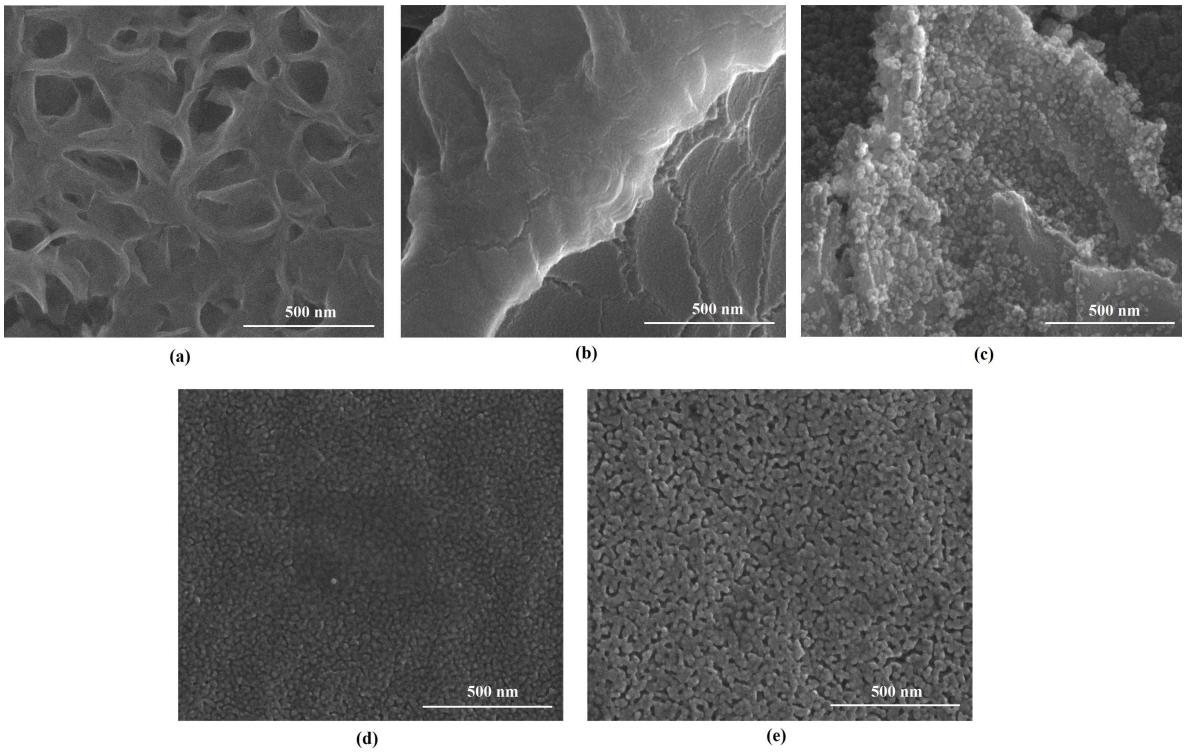

Fig. 6. SEM images of thin layers annealed at: (a) 393 K, (b) 573 K, (c) 673 K, (d) 773 K, and (e) 873 K at magnification 200k.

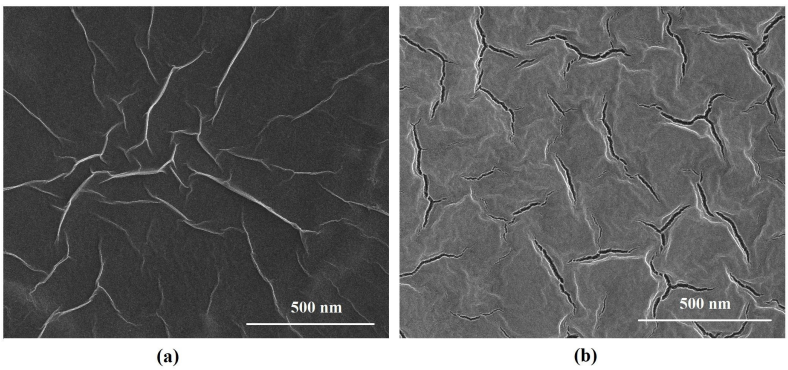

Fig. 7. SEM images of thin layers annealed at: (a) 773 K and (b) 873 K at magnification 10k.

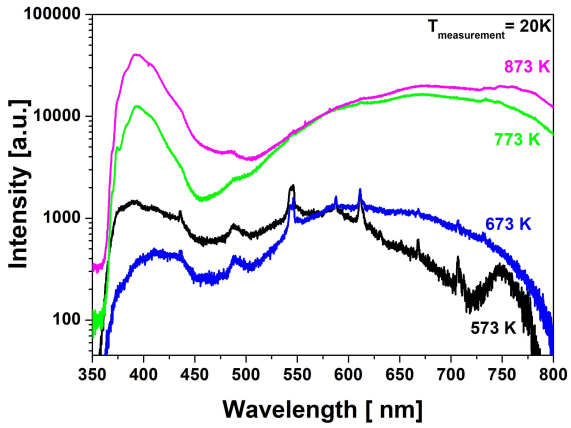

Fig. 8. Luminescence of studied thin layers measured at 20 K.

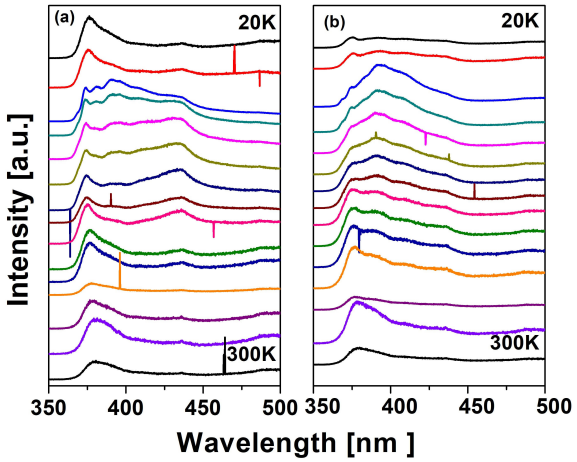

Fig. 9. Photoluminescence of a ZnO thin film annealed at (a) 773 K and (b) 873 K as a function of temperature (from 20 K to 300 K).

during production of a thin layer. Green emission is due to the recombination of electrons with holes trapped in free ionized oxygen vacancies. It should be mentioned that this emission is usually observed in ZnO which is synthesized in conditions of oxygen deficiency. Orange emission is less frequently described and its source, which is not completely understood, appears to include the presence of interstitial oxygen ions [48,49]. Thus, UV luminescence shows the quality of the crystal, while visible luminescence reveals structural defects.

Additionally, one can see that the exciton peak shifts towards lower wavelengths when the annealing temperature increases. We can also notice that the typical luminescence spectrum for zinc oxide is visible for films annealed at 773 K and 873 K. Whereas in the case of a thin layers annealed at 573 K and 673 K, the observed PL spectra are different. This is also confirmed by the results of the FTIR and Raman spectroscopy. We suppose that the increase in a particle size may cause the shift which is observed in the PL emission spectra. It is also possible that the decrease of an energy band gap of the studied materials as the annealing temperature increases can also shift the spectrum. It should be mentioned that the stress, which is generated in samples due to their annealing, can also affect the shift in the PL emission peak [50].

The optical properties of the semiconductor material can be controlled and modified by changing the amount and nature of defects. Defects are introduced during the growth process or after growth treatments such as annealing. ZnO has donor and acceptor energy levels below the conductivity band and above the valence band, respectively. They are responsible for emission on the edge of the NBE band (near-band-edge emission band). ZnO also has deep energy levels in the band with different energies that are responsible for emissions in the entire visible area from 400 nm to 750 nm. There are internal and external point defects and, both, contribute to luminescent properties of zinc oxide. Deep-level emission (DLE) band, in ZnO, has been attributed to various internal defects (such as oxygen vacancies, zinc vacancies, oxygen interstitial, zinc interstitial, oxygen anti-site, and zinc anti-site) in a ZnO crystal structure [51,52]. Figure 9 shows the examples of photoluminescence spectra of a ZnO thin layer deposited on a Si substrate, and, then, annealed at 773 K and 873 K. These spectra were measured in the range from 20 K to 300 K.

It can be seen that in this region the samples showed the emission related to excitons which discloses the quality of the thin layer. We found that with increasing temperature, the red shift of the peak occurs. This excitonic emission shift can be combined with a change in the localized level below the conduction band, as well as the carrier concentration above the valence band in the band gap [53,54]. It should be mentioned that the Varshni equation well characterizes the spectral shift of the exciton peak. This equation [see Eq. (6)] describes the band gap changes with temperature due to a crystal lattice thermal expansion [55].

Thermal evolution of the exciton peak in ZnO is shown in Fig. 10. One can see that this peak increases with increasing temperature to 75 K. This behavior may be associated with an increased thermal dissociation of bound excitons into free excitons with increasing temperature [56]. However, when the value of 75 K is reached, the peak intensity decreases. UV emission integral intensity decreases with increasing temperature because of the effect of a thermal quenching. This temperature dependence on excitons intensity may be used to determine the activation energy according to the equation:

$$I(T) = \frac{I_0}{1+Aexp\left(\frac{-E_a}{k_B T}\right)}, \tag{5}$$

where I_0 is the integral intensity at $T = 0$ K, A is the constant, E_a is the activation energy in the process of thermal quenching and k_B is the Boltzmann constant.

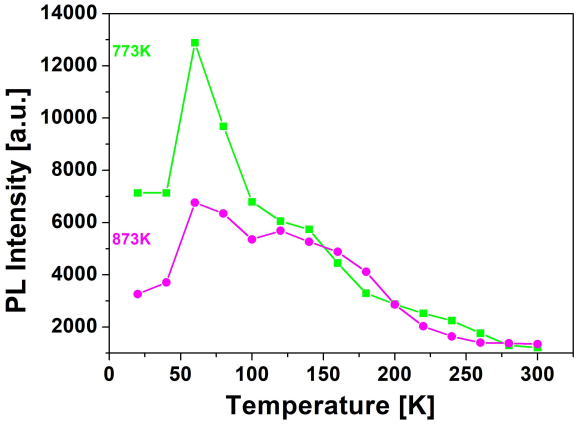

Fig. 10. Thermal evolution of a yellow-orange emission band in ZnO.

The inverse temperature dependence on logarithm of the UV emission integral intensity is shown in Fig. 11. Solid line presents the theoretical fit to the experimental data. From this fitting, we estimated the energy activation value as 14.6 meV for 773 K and 20.9 meV for 873 K. The obtained values are similar to these reported elsewhere [56,57].

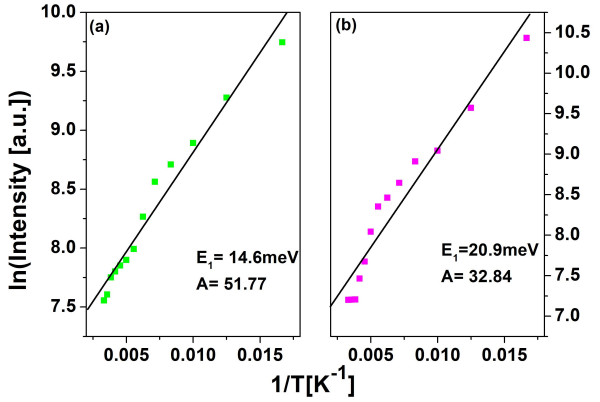

Fig. 11. Logarithm of the UV emission integral intensity as a function of 1/T.

Figure 12 presents the exciton peak energy as a function of temperature. The solid line shows the fit of the well-known Varshni equation [58]:

$$E_g(T) = E_g(0) - \frac{\alpha T^2}{\beta + T}, \quad (6)$$

where $E_g(0)$ is the energy band gap at $T = 0$, α and β are called the Varshini parameters, and, additionally, β is the proportional to the Debye temperature. For studied ZnO thin films, the matching parameters obtained are as follows: $E_g(0) = 3.326$ eV, $\alpha = 0.00072$ eV/K for 773 K and $E_g(0) = 3.322$ eV, $\alpha = 0.00089$ eV/K for 873 K. Whereas the β parameter was assumed as 920 K for a sample annealed at 773 K and 873 K [59,60]. All obtained values are consistent with those found elsewhere [60-63]. It should be mentioned that the existence of the free exciton just below the gap influences this energy gap. Thus, the gap value, which is determined using this method, is characterized by a considerable uncertainty and should be treated as a lower limit of its value [64].

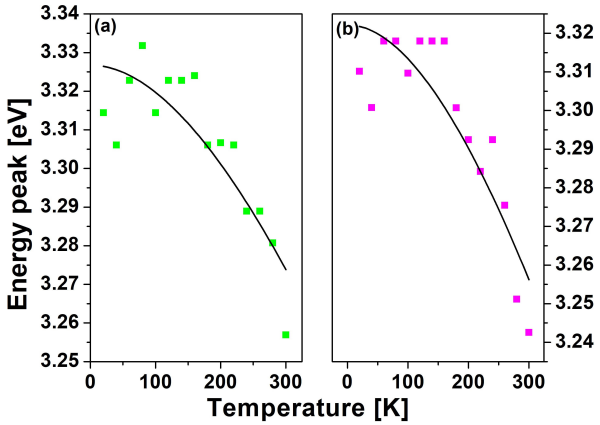

Fig. 12. Temperature dependence of the exciton energy peak for ZnO thin layers annealed at (a) 773 K and (b) 873 K fitted with the Varshni equation.

4. Conclusions

Thin films were prepared on silicon substrates using a rapid sol-gel method by a spin-coating technique. Sample were annealed at various temperatures in the range of 573–873 K. The characteristic (Zn–O) band at ~401–419 cm^{-1} is present in FTIR measurements for samples annealed at temperatures above 573 K. From FTIR and Raman measurements we can say that the pure zinc oxide is obtained for samples annealed at temperatures above 673 K. Organic residues (e.g. wide band 3000–3650 cm^{-1}) in the Raman spectrum are visible for the sample heated at lower temperatures. SEM measurements of studied thin films show that an increase in grain size was observed due to the increase in annealing temperature. We found that as the temperature increases, the grain size increases from 17 nm to 30 nm. From luminescence measurements one can see that all samples showed two dominant peaks. The excitonic peak reveals the quality of ZnO thin films. Whereas the second peak, which can be observed in visible region, displays structural defects. Additionally, we found that the excitonic peak shifts towards longer wavelengths as the temperature increases.

We found that the annealing temperature is important for luminescent and morphological properties of the studied layers. All presented results show that the zinc oxide layers were obtained for the samples annealed at 773 K and 873 K. While at lower temperatures and with the IR spectra accordance, the obtained thin films cannot be defined as a pure zinc oxide phase. We found that annealing temperature significantly affected crystallinity of the thin films.

Authors' statement

Research concept and design, R. Sz, and B. D.-Z.; collection and assembly of data, M. S; data analysis and interpretation, M. S; writing the article, M. S.; critical revision of the article, R. Sz. and B. D.-Z.; final approval of article, R. Sz., P. P., K. S. and B. D.-Z.

References

[1] Özgür, Ü. *et al.* A comprehensive review of ZnO materials and devices. *J. Appl. Phys.* **98,** 1–105 (2005). https://doi.org/10.1063/1.1992666

[2] Khan, Z. R., Khan, M. S. & Zulfequar, M. Optical and Structural Properties of ZnO Thin Films Fabricated by Sol-Gel Method. *Mater. Sci. Appl.* **2**, 340–345 (2011). https://doi.org/10.4236/msa.2011.25044

[3] Shen, W., Zhao, Y. & Hang, C. The preparation of ZnO based gas-sensing thin films by ink-jet printing method. *Thin Solid Films* **483,** 382–387 (2005). https://doi.org/10.1016/j.tsf.2005.01.015

[4] Fan, J. & Frezer, R. The roles played by Ag and Al dopants in controlling the electrical properties of ZnO varistors. *J. Appl. Phys.* **77,** 4795–4800 (1995). https://doi.org/10.1061/1.359398

[5] Szuszkiewicz, W. & Dynowska, E. Are values of parameters describing magnetic properties of crystal really fixed? *J. Alloys Compd.* **401,** 272–280 (2005). https://doi.org/10.1016/j.jallcom.2005.02.048

[6] Klingshirn, C. ZnO: Material, Physics and Applications. *Chem. Phys. Chem.* **8,** 82–803 (2007). https://doi.org/10.1002/cphc.200700002

[7] Morkoc, H. & Ozgur, U. *Zinc oxide: materials preparation, properties and devices.* (WILEY: New York, 2008). https://doi.org/10.1002/9783527623945

[8] Ellmer, K. & Mientus, R. Carrier transport in polycrystalline ITO and ZnO:Al II: The influence of grain barriers and boundaries. *Thin Solid Films* **516,** 5829–5835 (2008). https://doi.org/10.1016/j.tsf.2007.10.082

[9] Kim, H. *et al*. Transparent conducting aluminium-doped zinc oxide thin films for organic light-emitting devices. *Appl. Phys. Lett.* **76,** 259–261 (2000). https://doi.org/10.1063/1.125740

[10] Hoffman, R. L., Norris, B. J. & Wager, J. F. ZnO-based transparent thin-film transistors. *Appl. Phys. Lett.* **82,** 733–735 (2003). https://doi.org/10.1063/1.1542677

[11] Kulyk, B. *et al*. Structural Properties and Temperature Behaviour of Optical Absorption Edge in Polycrystalline ZnO:X (Cu,Ag) Films. *Acta Phys. Pol. A* **123**, 92–97 (2013). https://doi.org/10.12693/APhysPolA.123.92

[12] Abed, S. *et al*. Nonlinear optical properties of zinc oxide doped bismuth thin films using Z-scan technique. *Opt. Mater.* **56,** 40–44 (2016). https://doi.org/10.1016/j.optmat.2015.12.014

[13] Waszkowska, K. *et al*. Influence of ZnO nanoparticles on nonlinear optical properties of auronebased polymeric thin films. *Appl. Nanosci.* (2020). https://doi.org/10.1007/s13204-020-01373-3

[14] Tsukazaki, A. *et al*. Repeated temperature modulation epitaxy for p-type doping and light-emitting diode based on ZnO. *Nature Mater.* **4**, 42–46 (2005). https://doi.org/10.1038/nmat1284

[15] Farooqi, M. M. H. & Srivastava, R. K. Effect of Annealing Temperature on Structural, Photoluminescence and Photo-conductivity Properties of ZnO Thin Film Deposited on Glass Substrate by Sol–Gel Spin Coating Method. *Proc. Natl. Acad. Sci. India Sect. A Phys. Sci.* (2019) https://doi.org/10.1007/s40010-019-00648-x

[16] Tiwari, A. & Sahay, P. P. Sn–Ga co-doping in sol-gel derived ZnO thin films: Studies of their microstructural, optical, luminescence and electrical properties. *Materials Science in Semiconductor Processing* **118**, 105178-1 –105178-9 (2020). https://doi.org/10.1016/j.mssp.2020.105178

[17] Rhouma, F. I. H. *et al*. The structure and photoluminescence of a ZnO phosphor synthesized by the sol gel method under praseodymium doping. *RSC Adv.* **9**, 5206–5217 (2019). https://doi.org/10.1039/C8RA09939A

[18] Natsume, Y. & Sakata, H. Electrical and optical properties of zinc oxide films post-annealed in H2 after fabrication by sol-gel process. *Mater. Chem. Phys.* **78,** 170–176 (2002). https://doi.org/10.1016/S0254-0584(02)00314-0

[19] Luna-Arredondo, E. J. *et al*. Indium-doped ZnO thin films deposited by the sol-gel technique. *Thin Solid Films* **490,** 132–136 (2005). https://doi.org/10.1016/j.tsf.2005.04.043

[20] Farley, N. R. *et al*. Sol-gel formation of ordered nanostructured doped ZnO films, *J. Mater. Chem.* **14,** 1087–1092 (2004). https://doi.org/10.1039/B313271D

[21] Barwiolek, M., Szczęsny, R. & Szłyk, E. Copper(II) Schiff base complexes and their mixed thin layers with ZnO nanoparticles. *J. Chem. Sci.* **128,** 1057–1066 (2016). https://doi.org/10.1007/s12039-016-1116-y

[22] Abed, S. *et al*. Influence of concentration of nano particles of Bi on the electrical and optical properties of ZnO thin films. *Superlattices Microstruct.* **85,** 370–378 (2015). https://doi.org/10.1016/j.spmi.2015.06.008

[23] Sofiani, Z. *et al*. Third harmonic generation in undoped and X doped ZnO films (X: Ce, F, Er, Al, Sn) deposited by Spray Pyrolysis. *J. Appl. Phys.* **101,** 063104 (2007). https://doi.org/10.1063/1.2711143

[24] Figà, V., Derbal Habak H., Kulyk B. & Abbate M. Fluorescence Quenching in Hybrid Solar Cells Based on Electrodeposited ZnO, *J. Optoelectron. Adv. Mater*. **15**, 954–959 (2013).

[25] Anand V.K., Sood, S.C. & Sharma, A. Characterization of ZnO Thin Film Deposited by Sol-Gel Process. *AIP Conference Proceedings* **1324**, 399–401 (2010). https://doi.org/10.1063/1.3526243

[26] Speaks, D. T. Effect of concentration, aging, and annealing on sol gel ZnO and Al-doped ZnO thin films. *International Journal of Mechanical and Materials Engineering* **15,** 1–14 (2020). https://doi.org/10.1186/s40712-019-0113-6

[27] Dislich, H. Sol-gel: science, processes and products. *J. Non-Cryst. Solids* **80,** 115–121 (1986). https://doi.org/10.1016/0022-3093(86)90384-4

[28] Yang, C. Y., Pan, F., Zeng, F. & Liu, M. Switching mechanism transition induced by annealing treatment in nonvolatile Cu/ZnO/Cu/ZnO/Pt resistive memory: From carrier trapping/detrapping to electrochemical metallization. *J. Appl. Phys.* **106,** 1–4 (2009). https://doi.org/10.1063/1.3273329

[29] Danks, A. E., Hall, S.R. & Schnepp, Z. The evolution of sol-gel chemistry as a technique for materials synthesis. *Mater. Horiz.* **3**, 91–112 (2016). https://doi.org/10.1039/C5MH00260E

[30] Bahadur, H., Srivastava, A. K., Sharma, R. K. & Chandra, S. Morphologies of Sol-Gel Derived Thin Films of ZnO Using Different Precursor Materials and their Nanostructures. *Nanoscale Res. Lett.* **2**, 469–475 (2007). https://doi.org/10.1007/s11671-007-9089-x

[31] Sahal, M., Hartiti, B., Ridah, A., Mollar, M., Marı, B. Structural, electrical and optical properties of ZnO thin films deposited by sol-gel method. *Microelectron. J.* **39,** 1425–1428 (2008). https://doi.org/10.1016/j.mejo.2008.06.085

[32] Miller, J. B., Hsin-Jung, H. & Howard, B. H. Microstructural evolution of sol-gel derived ZnO thin films. *Thin Solid Films* **518,** 6792–6798 (2010). https://doi.org/10.1016/j.tsf.2010.06.032

[33] Murali, K. R. Properties of sol-gel dip-coated zinc oxide thin films. *J. Phys. Chem. Solids* **68,** 2293–2296 (2007). https://doi.org/10.1016/j.jpcs.2007.06.006

[34] Hosseini Vajargah, P., Abdizadeha, H., Ebrahimifard, R. & Golobostanfard, M. R. Sol-gel derived ZnO thin films: Effect of amino-additives. *Appl. Surf. Sci.* **285,** 732–743 (2013). https://doi.org/10.1016/j.apsusc.2013.08.118

[35] Brinker, C. J. & Scherer, G. W. *Sol-gel science: the physics and chemistry of sol-gel processing*. (Academic Press: Boston USA, 1990). https://doi.org/10.1016/B978-0-08-057103-4.50006-4

[36] Znaidi, L., Soler-Illia, G. J., Le Guennic, R., Kanaev, A. & Sanchez, C. Elaboration of ZnO Thin Films with Preferential Orientation by a Soft Chemistry Route. *J. Sol-Gel Sci. Tech.* **26,** 817–821 (2003). https://doi.org/10.1023/A:1020795515478

[37] Sakthivel, S. *et al*. Solar photocatalytic degradation of azo dye: comparison of photocatalytic efficiency of ZnO and TiO2. *Sol. Energy Mater. Sol. Cells* **77,** 65–82 (2003). https://doi.org/10.1016/S0927-0248(02)00255-6

[38] Popielarski, P. *et al*. Persistent photoconductivity in ZnO thin films grown on Si substrate by spin coating method. *Opt. Mater.* **97**, 109343 (2019). https://doi.org/10.1016/j.optmat.2019.109343

[39] Lopez-Mena, E., Jimenez-Sandowal, E. & Jimenez-Sandowal, O. ZnO thin films prepared at low annealing temperatures, from a novel, simple sol-gel precursor solution. *J. Sol- Gel Sci. Technol.* **74,** 419–424 (2015). https://doi.org/10.1007/s10971-014-3612-1

[40] Prasada Rao, T. & Santhoshkumar, M.C. Effect of thickness on structural, optical and electrical properties of nanostructured ZnO thin films by spray pyrolysis. *Appl. Surf. Sci.* **255,** 4579–4584 (2009). https://doi.org/10.1016/j.apsusc.2008.11.079

[41] Sendi, R. K. & Mahmud, S. Stress control in ZnO nanoparticle-based discs via high-oxygen thermal annealing at various temperatures. *J. Phys. Sci.* **24,** 1–15 (2013).

[42] Hong, R., Huang, J., He, H., Fan, Z. & Shao, J. Influence of different post-treatments on the structure and optical properties of zinc oxide thin films. *Appl. Surf. Sci.* **242,** 346–352 (2005). https://doi.org/10.1016/j.apsusc.2004.08.037

[43] Rusu, D. I., Rusu, G.G. & Luca, D. Structural characteristics and optical properties of thermally oxidized zinc films. *Acta Phys. Pol. A* **119,** 850–856. (2011) https://doi.org/10.12693/APhysPolA.119.850

[44] Popielarski, P. *et al*. Raman and impedance spectroscopy of blend polycarbonate and Zinc Oxide layers grown by sol-gel method. *Solid State Phenom.* **200,** 22–26 (2013). https://doi.org/10.4028/www.scientific.net/SSP.200.22

[45] Bala, W. *et al*. Optical and electrical properties of ZnO thin films grown by sol-gel method. *Solid State Phenom.* **200,** 14–21 (2013). https://doi.org/10.4028/www.scientific.net/SSP.200.14

[46] Yahiaa, B., Znaidi, L., Kanaeva, A. & Petitet, J. P. Raman study of oriented ZnO thin films deposited by sol-gel method. *Spectrochim. Acta A* **71**, 1234–1238 (2008). https://doi.org/10.1016/j.saa.2008.03.032

[47] Russo, V., Ghidelli, M., Gondoni, P., Casari, C. S. & Li Bassi, A. Multi-wavelength Raman scattering of nanostructured Al-doped zinc oxide. *J. Appl. Phys.* **115,** 073508 (2014). https://doi.org/10.1063/1.4866322

[48] Yi, S. H., Choi, S. K., Jang, J. M., Kim, J. A. & Jung, W. G. Low-temperature growth of ZnO nanorods by chemical bath deposition. *J. Colloid Interface Sci.* **313,** 705–710 (2007). https://doi.org/10.1016/j.jcis.2007.05.006

[49] Kashif, M. *et al*. Effect of different seed solutions on the morphology and electrooptical properties of ZnO nanorods. *J. Nanomater.* **2012,** 1–6 (2012). https://doi.org/10.1155/2012/452407

[50] Ungula, J., Dejene, B. F. & Swart, H. C. Effect of annealing on the structural, morphological and optical properties of Ga-doped ZnO nanoparticles by reflux precipitation method. *Results Phys.* **7** 2022–2027 (2017). https://doi.org/10.1016/j.rinp.2017.06.019

[51] Gomi, M., Oohira, N., Ozaki, K. & Koyano, M. Photoluminescent and structural properties of precipitated ZnO fine particles. *Japan. J. Appl. Phys.* **42,** 481–485 (2003). https://doi.org/10.1143/JJAP.42.481

[52] Janotti, A. & Van de Walle, C. G. Native point defects in ZnO. *Phys. Rew. B* **76,** 165202 (2007). https://doi.org/10.1103/PhysRevB.76.165202

[53] Abrarov, S. M., Yuldashev, Sh. U., Kim, T. W., Kwon, Y. H. & Kang, T.W. Deep level emission of ZnO nanoparticles deposited inside UV opal. *Opt. Commun.* **259,** 378–384 (2005). https://doi.org/10.1016/j.optcom.2005.08.048

[54] Sedky, A., Mossad Ali, A. & Mohamed, M. Structural and optical investigation of pure and Al doped ZnO annealed at different temperatures. *Opt. Quantum Electron.* **52:42**, 1–21 (2020). https://doi.org/10.1007/s11082-019-2158-4

[55] Wang, Z. M. *MoS2: Materials, Physics, and Devices*. (Springer: 2014). https://doi.org/10.1007/978-3-319-02850-7_8

[56] Kukreja, L. M. & Misra, P. Photoluminescence Processes in ZnO Thin Films and Quantum Structures. In *ZnO Nanocrystals and Allied Materials*. (Springer 2014). https://doi.org/10.1007/978-81-322-1160-0_3

[57] Kapustianyk, V. *et al*. Exciton spectra on the nanostructured zinc oxide. *J. Phys. Studies* **12,** 2602 (2008).

[58] Varshni, Y. P. Temperature dependence of the energy gap in semiconductors. Physica **34,** 149–154 (1967). https://doi.org/10.1016/0022-3697(79)90162-8

[59] Kulyk, B., Kapustianyk, V., Tsybulskyy, V., Krupka, O. & Sahraoui, B. Optical properties of ZnO/PMMA nanocomposite films. *J. Alloys Compd.* **502,** 24–27 (2010). https://doi.org/10.1016/j.jallcom.2010.04.162

[60] Rodnyi, P. A. & Khodyuk, I. V. Optical and Luminescence Properties of Zinc Oxide (Review). *Opt. Spektrosk.* **111,** 814-824 (2011). https://doi.org/10.1134/S0030400X11120216

[61] Hur, T. B., Jeen, G. S., Hwang, Y. H. & Kim, K. Photoluminescence of polycrystalline ZnO under different annealing conditions. *J. Appl. Phys.* **94,** 5786-5790 (2003). https://doi.org/10.1063/1.1617357

[62] Bundesmann, C., Schmidt-Grund, R. & Schubert, M. *Transparent Conductive Zinc Oxide: Basics and Application in Thin Film Solar Cells*. (Springer: Berlin, 2008). https://doi.org/10.1007/978-3-540-73612-7

[63] Ellmer, K. *Transparent conductive zinc oxide and its derivatives*. In *Handbook of Transparent Conductors*. (Springer: New York, NY, USA, 2011). https://doi.org/10.1007/978-1-4419-1638-9_7

[64] Rai, R.C., Guminiak, M., Wilser, S., Cai, B. & Nakarmi, M. L. Elevated temperature dependence of energy band gap of ZnO thin films gown by e-beam deposition. *J. Appl. Phys.* **111,** 073511 (2012). https://doi.org/10.1063/1.3699365